Copper(II) carboxylates with 2-aminopyridine. Synthesis, characterization and a study of the dimer–monomer equilibrium in acetonitrile solutions by VIS-spectroscopic and microcalorimetric titrations

Nina Lah,[a] Gerald Giester,[b] Jurij Lah,[a] Primož Šegedin[a] and Ivan Leban[a]

[a] *University of Ljubljana, Faculty of Chemistry and Chemical Technology, Aškerčeva 5, P.O. Box 537, SI-1001 Ljubljana, Slovenia. E-mail: nina.lah@uni-lj.si; Fax: +386 14258 220*
[b] *University of Vienna, Institute of Mineralogy and Crystallography, Althanstrasse 14, A-1090 Vienna, Austria*

Received (in Cambridge, UK) 5th December 2000, Accepted 8th February 2001
First published as an Advance Article on the web 30th March 2001

A series of copper(II) carboxylates with 2-aminopyridine was prepared. In all cases typical dinuclear complexes with a paddle-wheel type structure, $Cu_2X_4L_2$, as well as mononuclear complexes of type CuX_2L_2 were obtained (X = hexanoate, heptanoate, octanoate or nonanoate, L = 2-aminopyridine). The structures of monoclinic $Cu_2(O_2CC_7H_{15})_4(C_5H_6N_2)_2$, **1**, and $Cu(O_2CC_7H_{15})_2(C_5H_6N_2)_2$, **2**, were determined by X-ray diffraction. VIS-absorption spectroscopic and isothermal calorimetric titrations, were employed to investigate the dimer–monomer equilibrium in acetonitrile solutions. The results were analysed on the basis of the mass-action model to obtain the equilibrium constants of monomer formation ($K_M \approx 10^4$ L mol^{-1}). The thermodynamic analysis shows that for all studied systems monomer formation is an enthalpy-driven process ($\Delta H^\circ_M \approx -14$ kJ mol^{-1}). The observed exothermic ΔH°_M values result most likely from the attractive coordinative interactions between Cu^{2+} ion and 2-aminopyridine.

Introduction

The chemistry of copper(II) carboxylate complexes, especially with N-donor ligands, has been extensively studied over the past few decades.[1–5] Certain complexes have shown properties important for applications in diverse areas such as pharmaceuticals, fungicides, catalysts, gas occlusion compounds, and solvent extraction processes. Moreover, the attention of, bioinorganic chemists has been directed towards the synthesis and characterization of new copper(II) carboxylates with N-donor ligands to model the active sites in metallozymes.[6,7]

Our interest in copper(II) carboxylates containing different ligands originates from the fact that compounds of this type can potentially be used as wood preservatives. In our previous work an attempt was made to prepare compounds with increased fungicidal activity.[8,9] In continuation, a series of copper(II) complexes with carboxylates of different chain length [hexanoate (hex), heptanoate (hep), octanoate (oct), nonanoate (non)] with 2-aminopyridine (2-apy) was prepared. After the addition of small amounts of 2-aminopyridine to solutions of polymeric copper(II) carboxylates in acetonitrile green dimeric forms were obtained. By increasing the ligand concentration the solutions changed from green to blue and at higher ligand : copper molar ratio the blue monomeric form, prevailed. It was also noticed that with increasing hydrocarbon chain length the ligand concentration necessary for obtaining the pure monomeric form increased slightly. Our interest was concentrated on determining the driving force for the monomer formation. By using VIS-absorption spectroscopy and isothermal titration microcalorimetry we tried to evaluate the thermodynamic parameters of the monomer formation process and thus explain the qualitative observations obtained during the synthesis.

Experimental

Syntheses of the complexes were carried out using commercially available chemicals and solvents. For all syntheses the starting polymeric copper carboxylates were prepared by direct metathesis of the corresponding sodium soap in a slightly acidic aqueous solution with the required amount of copper sulfate.[1] The obtained copper carboxylates were purified by recrystallization from methanol.

Preparations

Bis(2-aminopyridine)tetrakis(μ-hexanoato-*O*,*O*′)dicopper(II). 2-Aminopyridine (0.1 g, 1.0 mmol) was added to a hot acetonitrile solution (15 mL) containing $Cu_2(O_2CC_5H_{11})_4$ (0.295 g, 0.5 mmol), and stirred at boiling temperature for 5 minutes. The resulting solution was cooled to ambient temperature and then left in a refrigerator overnight to precipitate the green product in average yield 53%. Calc. for $C_{12}H_{28}CuN_2O_4$: C, 52.63; H, 7.27; N, 7.22. Found: C, 52.70, H, 7.35; N, 7.29%. IR: $\upsilon_{asym}(CO_2)$ 1603, $\upsilon_{sym}(CO_2)$ 1420 cm^{-1}.

Dimeric complexes containing heptanoate, octanoate and nonanoate were obtained using the same procedure, only using different amounts of solvent. Calc. for $C_{19}H_{32}CuN_2O_4$: C, 54.85, H, 7.75, N, 6.73. Found: C, 54.85, H, 7.92, N, 6.98%. IR: $\upsilon_{asym}(CO_2)$ 1602, $\upsilon_{sym}(CO_2)$ 1423 cm^{-1}. Calc. for $C_{21}H_{36}CuN_2O_4$: C, 56.80; H, 8.17; N, 6.30. Found: C, 56.86, H, 8.30, N, 6.45%. IR: $\upsilon_{asym}(CO_2)$ 1602, $\upsilon_{sym}(CO_2)$ 1417 cm^{-1}. Calc. for $C_{23}H_{40}CuN_2O_4$: C, 58.51; H, 8.54; N, 5.93. Found: C, 58.76; H, 8.87; N, 6.21%. IR: $\upsilon_{asym}(CO_2)$ 1603, $\upsilon_{sym}(CO_2)$ 1415 cm^{-1}.

Bis(2-aminopyridine)Bis(hexanoato-*O*)copper(II). The procedure for obtaining the monomeric forms of the complexes was similar to that described for the dimers except that higher

amounts of the ligand (2-aminopyridine) were used. Calc. for $C_{22}H_{34}CuN_4O_4$: C, 54.81; H, 7.11; N, 11.62. Found: C, 54.85; H, 7.20; N, 11.71%. IR: $\upsilon_{asym}(CO_2)$ 1572, $\upsilon_{sym}(CO_2)$ 1403 cm^{-1}. Calc. for $C_{24}H_{38}CuN_4O_4$: C, 56.51; H, 7.51; N, 10.98. Found: C, 56.54; H, 7.70; N 11.02%. IR: $\upsilon_{asym}(CO_2)$ 1573, $\upsilon_{sym}(CO_2)$ 1402 cm^{-1}. Calc. for $C_{26}H_{42}CuN_4O_4$: C, 58.02; H, 7.86; N, 10.41. Found: C, 58.10; H, 8.03; N, 10.51%. IR: $\upsilon_{asym}(CO_2)$ 1571, $\upsilon_{sym}(CO_2)$ 1402 cm^{-1}. Calc. for $C_{28}H_{46}CuN_4O_4$: C, 59.39; H, 8.19; N, 9.89. Found: C, 59.33; H, 8.29; N, 9.98%. IR: $\upsilon_{asym}(CO_2)$ 1570, $\upsilon_{sym}(CO_2)$ 1402 cm^{-1}.

Vibrational spectra were measured in the region 4000 to 400 cm^{-1} with a Perkin-Elmer FT-IR 1720X spectrophotometer using Nujol and poly(chlorotrifluoroethylene) oil suspension techniques. Only selected data are given; complete data can be obtained on request.

X-Ray crystallography

Suitable single crystals of $Cu_2(oct)_4(2\text{-apy})_2$ were obtained by slow evaporation of an acetonitrile solution at room temperature, those of $Cu(oct)_2(2\text{-apy})_2$ directly from the reaction solution after standing for two days in a refrigerator at 10 °C. The diffraction experiments were carried out on a Nonius Kappa CCD diffractometer with Mo-Kα radiation (0.710 73 Å). The relevant crystal data and structure parameters are summarized in Table 1. The structure solutions and full matrix least-squares refinements based on F^2 were performed with the SHELXS 97 and SHELXL 97 program packages.[10] Non-hydrogen atoms were refined anisotropically. Hydrogen atoms were generated geometrically, assigned appropriate isotropic thermal displacement parameters and allowed to ride on their parent atoms.

CCDC reference numbers 159070 and 159071. See http://www.rsc.org/suppdata/nj/b0/b009807h/ for crystallographic data in CIF or other electronic format.

VIS-Absorption spectrophotometry

Absorbance was measured with a Cary 1 UV spectrophotometer (Varian, Australia) equipped with a thermoelectrically controlled cell holder and cuvettes of 0.25 mm to 1 cm path length. VIS spectrophotometric titrations were conducted at 25 °C by incrementally injecting 4–8 μL aliquots of ligand (2-apy) acetonitrile solution into a dimer solution in the same solvent located in the cuvette of 1 cm path length. The concentrations of dimers (D) were 2 mmol L^{-1} while the concentrations of 2-apy were about 100 times higher. After each injection a VIS spectrum was recorded between 400 and 900 nm. Then the contribution of the dimer was subtracted from the measured spectra (Fig. 3A) to obtain the induced VIS spectrum of the monomer which was normalized to 1 mol L^{-1} dimer concentration (Fig. 3B).

Isothermal titration calorimetry (ITC)

The heats of monomer formation were measured by titration calorimetry performed with a TAM 2277 microcalorimeter (Thermometric AB, Sweden). For each measurement an acetonitrile solution of a given dimer (2 mL) was titrated at 25 °C with a 2-apy solution in the same solvent using a motor driven 250 μL syringe. The concentration of the dimer in the titration cell was 2 mmol L^{-1} for all experiments while the 2-apy concentration was about 50 times higher. In a single experiment ≈25 injections of 7 μL of the titrant solution were added to the titration cell. The reference cell of the microcalorimeter was filled with acetonitrile and the instrument calibrated by means of a known electrical pulse. The area under the peak that follows each injection is proportional to the resulting heat of monomer formation. The measured heat effects of 2-apy dilution were lower than the experimental error (≈50 μJ) and neglected. The integration of peaks from the directly recorded calorimetric plots (Fig. 4A) was performed using the Digitam program software (Thermometric AB, Sweden).

Analysis of signals accompanying titration experiments

The process of momomer (M) formation from dimer (D) and ligand (L) can be described according to the mass action model as in eqn. (1).

$$D + 2L \rightleftharpoons 2M, \quad K_M = [M]^2/[D][L]^2 \tag{1}$$

The quantities in square brackets are the corresponding equilibrium concentrations of components participating in the equilibrium in eqn. (1) and K_M is the monomer formation constant. According to this model the total added ligand concentration, $[L]_T$, and the total dimer concentration, $[D]_T$, can be presented as in eqn. (2).

$$[L]_T = [L] + [M] \quad \text{and} \quad [D]_T = [D] + \tfrac{1}{2}[M] \tag{2}$$

The process of monomer formation can be monitored by VIS-absorption spectroscopy. In accordance with the mass-action model [eqn. (1)] the measured absorption, A, can be expressed as in eqn. (3);

$$A = A_D + A_M + A_L \tag{3}$$

where A_D, A_M and A_L are the absorption contributions of D, M and L. Provided that for D and M the absorption is an

Table 1 Crystal data for $Cu_2(oct)_4(2\text{-apy})_2$ and $Cu(oct)_2(2\text{-apy})_2$

Empirical formula	$C_{42}H_{72}Cu_2N_4O_8$	$C_{26}H_{42}CuN_4O_4$
Formula weight/g mol^{-1}	888.1	538.2
T/K	100	200
Crystal system	Monoclinic	Monoclinic
Space group	$P2_1/a$	$P2_1/n$
a/Å	8.399(1)	8.427(2)
b/Å	14.738(2)	25.312(5)
c/Å	18.901(3)	13.734(3)
β/°	99.35(1)	105.42(3)
Z	2	4
μ/mm^{-1}	0.973	0.809
Reflections collected	6579	10858
Independent reflections	3839	5731
R_{int}	0.0376	0.0507
Final $R1$, $wR2$ [$I > 2\sigma(I)$]	0.055, 0.149	0.069, 0.131
(all data)	0.079, 0.174	0.129, 0.149

ideal concentration property (Beer–Lambert law is obeyed) and because the measured $A_L = 0$ in the wavelength range between 400 and 900 nm, by combining eqn. (2) and (3) one can express the measured A as in eqn. (4),

$$A = \varepsilon_D[D]_T l + \left\{\varepsilon_M - \frac{\varepsilon_D}{2}\right\}[M]l$$

$$= \varepsilon_D[D]_T l + \Delta\varepsilon_M[M]l \quad (4)$$

where ε_D and ε_M are the molar absorption coefficients of D and M, respectively, and l is the optical path length. If the contribution of D [the first term on the right-hand side of eqn. (3)] is subtracted from the measured A and the "difference absorbance" so obtained is normalized to the D unit concentration an expression for the "difference molar absorption coefficient", $\Delta\varepsilon$, is obtained, eqn. (5).

$$\Delta\varepsilon = \Delta\varepsilon_M[M]/[D]_T \quad (5)$$

As follows from eqn. (1), (2) and (5), the VIS-absorption titration curve is at given $[D]_T$ and varying $[L]_T$ described only in terms of parameters $\Delta\varepsilon_M$ and K_M. Their values were obtained by fitting the model function [eqn. (5)] to the experimental titration curve (Fig. 3C) using a weighted non-linear regression procedure based on minimization of the χ^2 function.[11–14]

In titration microcalorimetry experiments the measured property reflects the heat effect, q_i (see Fig. 4A), that results from each injection of titrant solution into the titration cell. The measured heat effect is usually given as the enthalpy change, ΔH, expressed per mol of added titrant, Δn_2 (Fig. 4B). As the amount of titrant added per injection, Δn_2, is very small, ΔH can be expressed as in eqn. (6)

$$\Delta H = \frac{q_i}{\Delta n_n} = \left(\frac{H_i - H_{i-1}}{\Delta n_2}\right)_{n_1, P, T} - \frac{H_a}{\Delta n_2} = \bar{H}_2 + \text{const.} \quad (6)$$

where H_i and H_{i-1} represent enthalpies of solution in the measuring cell after the ith and $(i-1)$th injection, respectively, H_a is the enthalpy of the added aliquot of the titrant solution and $\bar{H}_2$ the partial molar enthalpy of the added titrant in the solution in the titration cell.

The enthalpy of this solution after the ith injection according to the mass action approach [eqn. (1)] can be expressed as in eqn. (7)

$$H_i = n_1\bar{H}_1 + n_D\bar{H}_D + n_L\bar{H}_L + n_M\bar{H}_M \quad (7)$$

where n_1 is the amount of solvent, n_D the number of mol of D, n_L the number of mol of unassociated L and n_M the number of mol of the monomer M. $\bar{H}_1$, $\bar{H}_D$, $\bar{H}_L$, $\bar{H}_M$ are the corresponding partial molar enthalpies. It is easy to show that partial differentiation of eqn. (7) with respect to the total amount of added ligand, n_2, at constant P, T and n_1 combined with the Gibbs–Duhem equation leads to $\bar{H}_2$ expressed as in eqn. (8):[12]

$$\bar{H}_2 = \bar{H}_L + \frac{\Delta H_M}{2}\left(\frac{\partial n_M}{\partial n_2}\right)_{n_1, P, T} \quad (8)$$

where the enthalpy of monomer (M) formation, ΔH_M, defined as in eqn. (9)

$$\Delta H_M = 2\bar{H}_M - 2\bar{H}_L - \bar{H}_D \quad (9)$$

is the enthalpy change accompanying the process in which 2 mol of L and 1 mol of D are converted into 2 mol of monomer M. If one takes into account that the measured heat of dilution of L is so small that it can be neglected and assumes that $\Delta H_M = \Delta H_M^\circ$ and that $\bar{H}_L$ does not depend on the D concentration a well-known simple relation between the measured ΔH (eqn. 6) and ΔH_M° [eqn. (8) and (9)] emerges;[15] eqn. (10).

$$\Delta H = \frac{\Delta H_M^\circ}{2}\left(\frac{\partial n_M}{\partial n_2}\right)_{n_1, P, T} \quad (10)$$

The derivative in eqn. (8) for a given K_M can be expressed as a function of $[D]_T$ and $[L]_T$ [eqn. (1) and (2)] and therefore we were able to obtain K_M and ΔH_M° values by the already mentioned non-linear fitting of the model function [eqn. (10)] to the corresponding experimental ITC curve (Fig. 4B).[11–14]

Results and discussion

Description of the structures

Bis(2-aminopyridine)tetrakis(μ-octanoato-*O*,*O*′)dicopper(II). In the dimeric complex (Fig. 1) the copper ions are bridged by four octanoate ligands with the center of symmetry located between the copper ions. The square pyramidal coordination around each copper ion is completed by 2-aminopyridine in apical positions. Despite the presence of the NH_2 group 2-aminopyridine is coordinated through its endocyclic N atom. The copper ion is displaced from the plane consisting of four equatorial oxygen atoms toward the apical position by 0.215(6) Å. The copper–copper separation of 2.662(1) Å as well as other geometrical parameters (Table 2) are normal for this type of compound and comparable to the known structure of the complex containing acetate instead of octanoate.[17,18]

Within the molecule intramolecular hydrogen bonds of the N–H···O type are present; the remaining hydrogen atom from the NH_2 group is involved in intermolecular hydrogen bonds that link discrete dimeric units. Hydrocarbon chains of the octanoate ligand are not in the common zigzag conformation. One pair is distorted by rotation about C11–C12 only, while in the other pair distortions by rotation about C–C are much more severe. Distortions of the chains reduce the molecular volume and thus facilitate the packing in the crystal.

Bis(2-aminopyridine)bis(octanoato-*O*)copper(II). In the monomeric form (Fig. 2) the copper ion is six-coordinate (4 + 2); the 2-aminopyridine ligands are arranged *cis* to each other. Two pyridine N atoms and two carboxylate O atoms form a slightly tetrahedrally distorted square planar arrangement with two remaining carboxylate O atoms above and below the plane at much longer distances. The angle between the pyridine rings is 83.9(1)° and that between carboxylate groups 86.1(6)°. The molecular structure is similar to that of bis(acetato-*O*)bis(2-aminopyridine)copper(II),[19] although the

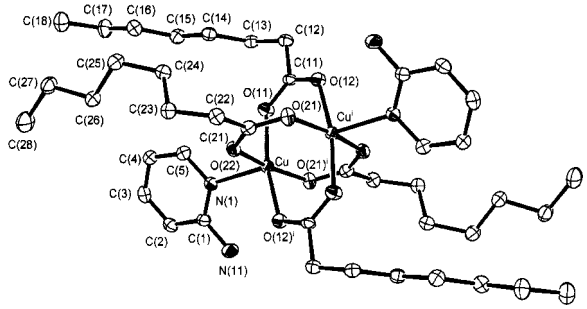

Fig. 1 ORTEP III[16] view of compound **1**. Thermal ellipsoids are drawn at the 50% probability level.

Table 2 Selected geometrical parameters (lengths in Å, angles in °) for $Cu_2(oct)_4(2\text{-apy})_2$ and $Cu(oct)_2(2\text{-apy})_2$

$Cu_2C_{42}H_{72}N_4O_8$			
Cu–O(11)	1.972(3)	Cu···Cu^{i}	2.662(1)
Cu–O(21)^{i}	1.950(3)	C(11)–O(11)	1.263(5)
Cu–O(12)^{i}	1.972(3)	C(11)–O(12)	1.258(5)
Cu–O(22)	1.970(3)	C(21)–O(21)	1.255(5)
Cu–N(1)	2.198(4)	C(21)–O(22)	1.271(6)
Hydrogen bonds	D···A	D–H–A	
N(11)···O(12)^{i}	3.030(5)	150.6	
N(11)···O(22)^{ii}	3.135(5)	158.0	
N(11)···O(12)^{iii}	3.142(5)	126.8	
Symmetry codes: i: $-x, -y, -z$; ii: $x+0.5, y-0.5, z$; iii: $-x+0.5, y-0.5, -z+2$.			
$CuC_{26}H_{42}N_4O_4$			
Cu–O(11)	1.977(3)	C(11)–O(11)	1.283(5)
Cu–O(12)	2.647(3)	C(11)–O(12)	1.241(5)
Cu–O(21)	1.957(3)	C(21)–O(21)	1.266(5)
Cu–O(22)	2.528(3)	C(21)–O(22)	1.244(6)
Cu–N(1)	1.990(3)		
Cu–N(2)	1.996(4)		
Hydrogen bonds	D···A	D–H–A	
N(11)···O(12)	2.984(5)	176.2	
N(11)···O(12)^{i}	2.901(4)	163.6	
N(21)···O(22)	2.953(6)	178.1	
N(21)···O(11)^{ii}	2.917(4)	157.8	
Symmetry codes: i: $-x, -y, -z$; ii: $-x, -y, -z+1$.			

two compounds crystallize in different space groups. The majority of mononuclear copper(II) carboxylates with amino and (or) methyl substituted pyridines in the 2 or 2 and 6 positions show a *trans* arrangement of ligands around the copper.[20] Beside the already mentioned compound only the complex bis(acetato-*O*)bis(2,6-diaminopyridine-*N*)copper(II) possesses a *cis* arrangement of ligands around the Cu.[21]

Both amino groups are involved in intramolecular hydrogen bonds to non-coordinated oxygen atoms of carboxylate groups. Molecules are connected into infinite chains along the *c* axis through additional hydrogen bonds also of a N–H···O type (for geometrical details see Table 2).

VIS-absorption spectroscopy

The existence of the two structure types (dimer and monomer) and the color change of the acetonitrile solution observed during the synthesis of monomer (M) [after addition of a certain amount of L to the solution that initially contained dimer (D)] led us to monitor the dimer–monomer equilibrium by VIS-absorption spectroscopy. VIS spectra for each of the studied systems were recorded in the wavelength range between 400 and 900 nm (Fig. 3A). The octanoate dimer (dashed line in Fig. 3A) shows two minima at 555 and 875 nm and one maximum at 695 nm. Almost identical spectra were observed with hexanoate, heptanoate and nonanoate dimers.

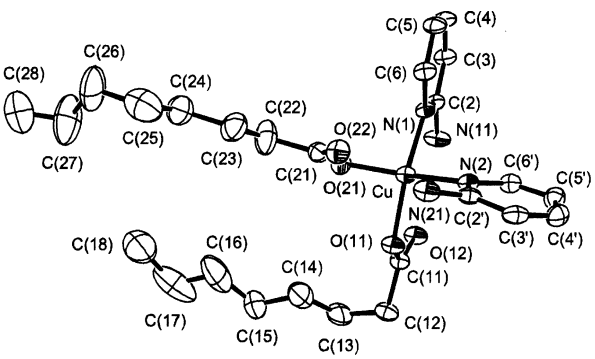

Fig. 2 ORTEP III view of compound **2**. Details as in Fig. 1.

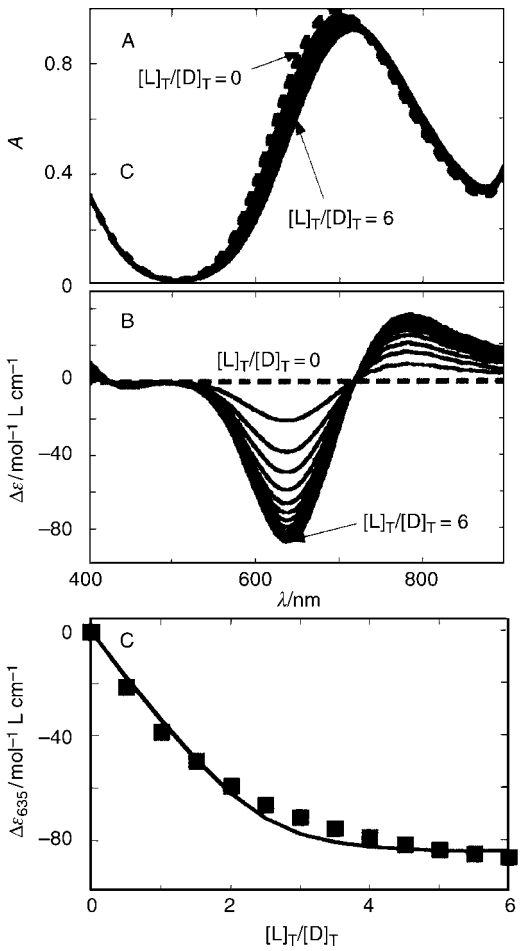

Fig. 3 Typical VIS-spectroscopic titration of octanoate with 2-aminopyridine in acetonitrile solution at 25 °C (panel A); $[D_T] = 2$ mM. The corresponding induced VIS difference spectra of octanoate monomer are shown in panel B and the VIS spectroscopic titration curve obtained at 635 nm as a function of $[L_T] : [D_T]$ ratio in C. The full line represents the best fit of the corresponding model function [eqn. (5)].

When the ligand was added to any of the studied dimer solutions the corresponding maximum was shifted to higher wavelengths while the positions of the minima stayed practically the same (Fig. 3A). The observed raw spectra were treated as sums of contributions of D and M species [eqn. (3)]. The corresponding difference molar absorption coefficients, $\Delta\varepsilon$, obtained by subtraction of the D contribution from the spectral signal [eqn. (4) and (5)] demonstrate similar characteristics for all the monomers formed. The absolute value of $\Delta\varepsilon$ increases more rapidly with the $[L]_T : [D]_T$ ratio up to $[L]_T : [D]_T \approx 2$, while beyond this value the increase becomes much slower (Fig. 3B). This behaviour indicates that in the monomer formation process from the corresponding dimer two L molecules are involved. The difference VIS spectra of hexanoate, heptanoate, octanoate and nonanoate monomers are almost identical and show one large minimum at 635 nm and one maximum at 782 nm (Fig. 3B). This observation suggests that the monomer formation for all studied systems is caused by the same type of interactions.

The χ^2 analysis of the VIS-spectroscopic titration curve for octanoate (Fig. 3C) shows that the model function [eqn. (5)] characterized by the formation constant, $K_M = 1.2 \times 10^4$ L mol^{-1}, fits the experimental one rather well. Good correlation between the model [eqn. (5)] and experiment is observed also with hexanoate, heptanoate and nonanoate. On the other hand, inspection of Table 3 demonstrates that the values of the formation constants decrease slightly with increasing carboxylate alkyl chain length. Owing to the low mean-square deviations of the K_M values (Table 3) this decrease of K_M may support the qualitative observation that with increasing carboxylate alkyl chain length a little bit more ligand is needed to obtain the same amount of monomer.

Titration calorimetry (ITC)

To get a deeper insight into the monomer formation process the dimer–monomer equilibrium was studied also by ITC. As an advantage over VIS-absorption spectroscopy, ITC provides direct access not only to the standard Gibbs free energy of monomer (M) formation, ΔG°_M, but also to the other two important thermodynamic quantities of monomer formation, standard enthalpy of monomer formation, ΔH°_M, and standard entropy of monomer formation, ΔS°_M. The directly recorded calorimetric signal (power *vs.* time) accompanying the monomer formation process (Fig. 4A) shows that after each injection of ligand solution into the solution in the titration cell (containing initially D) heat is emitted. The corresponding calorimetric titration curve for hexanoate presented in Fig. 4B indicates that the measured ΔH expressed per mol of added ligand decreases with increasing $[L]_T : [D]_T$ ratio. The titration curves for heptanoate, octanoate and nonanoate are of very similar shapes and magnitudes to the one observed with hexanoate. The values of K_M obtained from model analysis of the ITC curves (Table 3) tend to be somewhat lower then those derived from fitting of the VIS-spectroscopic titration curves. This is not unusual since much larger discrepancies in the values of the equilibrium constants obtained by different experimental methods have often been observed.[22–24]

Table 3 Monomer formation constants K_M for hexanoate, heptanoate, octanoate and nonanoate determined from the VIS-spectroscopic and ITC titration curves in acetonitrile solutions at 25 °C[a]

	K_M/(L mol^{-1})	
Carboxylate	VIS spectroscopy	ITC
Hexanoate	$(1.9 \pm 0.3) \times 10^4$	$(4.0 \pm 0.3) \times 10^3$
Heptanoate	$(1.5 \pm 0.2) \times 10^4$	$(3.6 \pm 0.2) \times 10^3$
Octanoate	$(1.2 \pm 0.2) \times 10^4$	$(3.1 \pm 0.2) \times 10^3$
Nonanoate	$(7 \pm 1) \times 10^3$	$(2.6 \pm 0.2) \times 10^3$

[a] The relative error in each titration point, $\Delta F/F$, is estimated to be $\pm 2\%$ for VIS spectroscopy ($F = \Delta\varepsilon$) and $\pm 5\%$ for ITC ($F = \Delta H$).

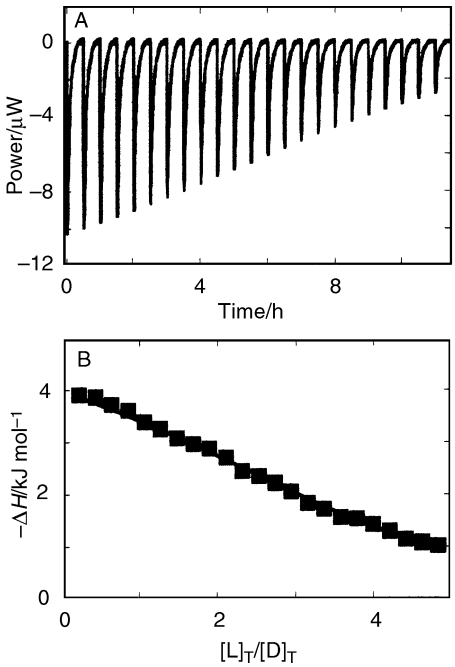

Fig. 4 Typical calorimetric (ITC) titration: 2 mL of an acetonitrile solution of hexanoate dimer were titrated with an acetonitrile solution of 2-aminopyridine (2×10^{-3} mol L^{-1}) at 25 °C. Each peak corresponds to a 7 μL injection of the titrant solution (panel A). The corresponding experimental and model (full line) titration curves are shown in panel B. ΔH values are expressed in kJ mol^{-1} of added ligand.

Thermodynamics of monomer (M) formation

The monomer formation can be discussed in terms of the following thermodynamic quantities: ΔG°_M, obtained as $-RT \ln K_M$, and ΔH°_M both determined from the ITC titration curves and ΔS°_M obtained from $\Delta G^\circ_M = \Delta H^\circ_M - T\Delta S^\circ_M$. The thermodynamic profiles of monomer formation for all measured dimer–monomer systems, determined at 25 °C, are presented in Fig. 5. These profiles show that the monomer formation for all studied carboxylates is an enthalpy driven process. The exothermic ΔH°_M values are most probably the consequence of the coordinative binding of the two 2-apy molecules to the Cu^{2+} ion.

We would also like to point out that the success of spectroscopic and microcalorimetric titrations in evaluating the thermodynamic parameters (K_M, ΔH°_M) characteristic for the monomer formation depends strongly on the shape of the titration curve that is fitted with the corresponding theoretical curve. To illustrate this dependence the simulations of the

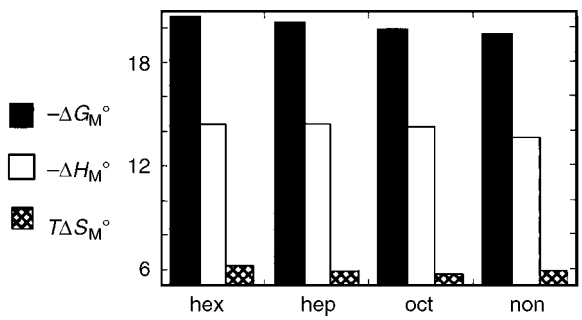

Fig. 5 Thermodynamic profiles for the hexanoate, heptanoate, octanoate and nonanoate monomer formation in acetonitrile solutions at 25 °C expressed in kJ mol^{-1}.

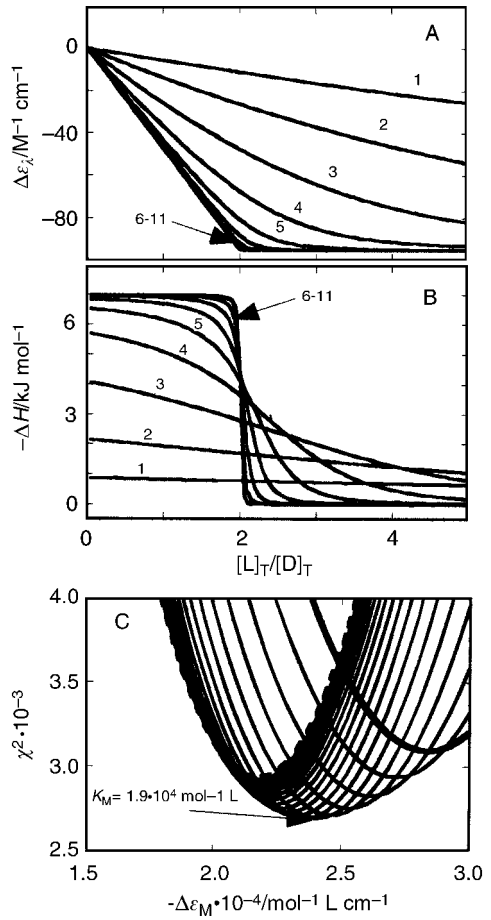

Fig. 6 The dependence of the simulated VIS-spectroscopic titration curve ($\Delta\varepsilon_M = -2.4 \times 10^4$ L mol^{-1} cm^{-1}; panel A) and the corresponding ITC curve ($\Delta H^\circ_M = -14$ kJ mol^{-1}; panel B) at log K_M varying between 1 and 11. Minimization of the χ^2 function over $\Delta\varepsilon_M$ at different K_M values varying between 10^3 (bold line) and 10^7 L mol^{-1} (dashed line) is shown in panel C.

VIS-spectroscopic and ITC titration curves performed for fixed linear parameters ($\Delta\varepsilon_M$, ΔH°_M) are presented in Fig. 6A and B. The simulation of VIS-spectroscopic titration curves for the selected (experimental) total dimer concentration, $[D]_T = 2$ mmol L^{-1}, shows that the curves follow changes in K_M up to 10^6 L mol^{-1} (Fig. 6A). Similar K_M dependence for the same total D concentration is observed also with ITC titration curves (Fig. 6B). In other words, the determination of K_M by minimization of the χ^2 function at given $[D]_T$ is possible only as long as the simulated curves show observable dependence on K_M, that is for $K_M < \approx 10^6$ L mol^{-1}. An example of such minimization is presented in Fig. 6C where it is shown that for the hexanoate dimer–monomer system a quite sharp minimum in the χ^2 function appears at $K_M = 1.9 \times 10^4$ L mol^{-1} and $\Delta\varepsilon_M = -2.38 \times 10^4$ L mol^{-1} cm^{-1}. Actually the shape of the curve depends on the $K_M[D]_T$ product which must be in the 1–1000 range.[15,22,25,26] Only if this requirement is fulfilled will the described fitting[15] of the experimental titration curves lead to reliable K_M values. It was shown that in the case of $K_M[D]_T < 1$ the parameters K_M and $\Delta\varepsilon_M$ (ΔH°_M) are too correlated while in the case of $K_M[D]_T >$ 1000 the mean-square deviation in K_M would be to high.[26] Evidently, a successful application of spectroscopic and calorimetric titrations depends on the K_M and $[D]_T$ values and on the magnitude of the measured signals used for monitoring the dimer–monomer equilibrium. Since the described titrations were performed within the appropriate concentration range ($[D]_T = 2$ mmol L^{-1}) and the measured signals were large enough we were able to analyse them in terms of the mass action model of monomer formation and the corresponding fitting procedures.

Conclusions

Although in many cases the reactions of copper(II) carboxylates with N-donor ligands produce only dimeric or monomeric complexes we succeeded in preparing and characterizing in the system of copper(II) carboxylates of different fatty acids and 2-aminopyridine both dinuclear and mononuclear complexes. To the best of our knowledge this is the first example where the combination of VIS-absorption spectroscopy and isothermal titration microcalorimetry has been applied to study the dimer–monomer equilibrium in solutions containing copper(II) carboxylates. The model analysis of VIS spectroscopic titration curves shows that monomer formation is most favorable in the case of hexanoate while with increasing copper(II) carboxylate alkyl chain length a slight lowering of the monomer formation constant is observed [K_M (hexanoate) $\approx 3\ K_M$ (nonanoate)].

The comparison between ΔH°_M and ΔS°_M values indicates that the monomer formation for hexanoate, heptanoate, octanoate and nonanoate complexes is an enthalpy driven process, most probably due to strong association between the two 2-apy molecules and the Cu^{2+} ion.

Finally, we used the VIS-absorption and ITC titration curves simulated on the basis of the mass action model to show the importance of the chosen initial experimental conditions (concentrations) and the K_M value in determining the thermodynamic parameters that describe the dimer–monomer equilibrium.

Raw data and details on calculation procedure can be obtained from the authors upon request.

Acknowledgements

The work was financially supported by The Ministry for Science and Technology, Republic of Slovenia, through grants J1-0442 and PS-511-103. We thank Professor Dr Gorazd Vesnaver for critical reading of the manuscript and many helpful suggestions.

References

1 R. C. Mehrotra and R. Bohra, *Metal Carboxylates*, Academic Press, London, 1983.
2 M. Melnik, *Coord. Chem. Rev.*, 1981, **36**, 1.
3 M. Melnik, *Coord. Chem. Rev.*, 1982, **47**, 234.
4 M. Kato and Y. Muto, *Coord. Chem Rev.*, 1988, **92**, 45.
5 M. R. Sundberg, R. Uggla and M. Melnik, *Polyhedron*, 1996, **15**, 1157.
6 J. Reedijk, W. L. Driessen, J. van Rijn, K. D. Karlin and J. Zubieta, (Editors), *Biological and Inorganic Copper Chemistry*, Adenine Press, New York, 1986, p. 143.
7 C. R. Holz, J. M. Bradshaw and B. Bennet, *Inorg. Chem.*, 1998, **37**, 1219, and references therein.
8 B. Kozlevčar, I. Leban, I. Turel, P. Šegedin, M. Petrič, F. Pohleven, A. J. P. White, D. J. Wiliams and J. Sieler, *Polyhedron*, 1999, **18**, 755.
9 B. Kozlevčar, N. Lah, I. Leban, I. Turel, P. Šegedin, M. Petrič, F. Pohleven, A. J. P. White and G. Giester, *Croat. Chem. Acta*, 1999, **72**, 427.
10 G. M. Sheldrick, SHELXS 97 and SHELXL 97, University of Göttingen, Germany, 1997.
11 W. H. Press, B. P. Flannery, S. A. Teukolsky and W. T. Vetterling, *Numerical Recepies*, Cambridge University Press, Cambridge, 1989.
12 J. Lah, C. Pohar and G. Vesnaver, *J. Phys. Chem. B*, 2000, **104**, 2522.
13 J. Lah and G. Vesnaver, *Biochemistry*, 2000, **39**, 9317.
14 J. Lah and G. Vesnaver, *Croat. Chem. Acta*, 2001, **74**, 37.
15 T. Wiseman, S. Willston, J. Brandts and L. Lin, *Anal. Biochem.*, 1989, **179**, 131.

16 ORTEP III, L. J. Farrugia, *J. Appl. Crystallogr.*, 1997, **30**, 565.
17 A. S. Antsiskhina, M. A. Porai-Koshits, V. N. Ostrikova, D. A. Garnovsky, A. P. Sadimenko and O. A. Osipov, *Koord. Khim.*, 1987, **13**, 836.
18 D. A. Garnovsky, A. P. Sadimenko, O. A. Osipov, A. S. Antsishkina and M. A. Porai-Koshits, *Inorg. Chim. Acta*, 1989, **160**, 177.
19 R. Grobelny, T. Glowiak, J. Mrozinski, L. Brzozka, W. Baran and P. Tomasik, *Pol. J. Chem.*, 1995, **69**, 559.
20 N. Lah, L. Golič, P. Šegedin and I. Leban, *Acta Crystallogr., Sect. C*, 1999, **55**, 1056.
21 B. Kozlevčar, N. Lah, K. Podlipnik and I. Leban, unpublished results.
22 C. Hu and J. M. Sturtevant, *J. Phys. Chem.*, 1992, **96**, 4052.
23 G. L. Bertrand, J. R. Faulkner, S. M. Han and D. W. J. Armstrong, *J. Phys. Chem.*, 1989, **93**, 6863.
24 H. Mwakibete, R. Cristantino, D. M. Bloor, E. Wyn-Jones and J. F. Holzwarth, *Langmuir*, 1995, **11**, 57.
25 D. J. Eatough, E. A. Lewis and L. D. Hansen, *Analytical Solution Calorimetry*, ed. K. J. Grime, John Wiley & Sons, New York, 1985, pp. 137–161.
26 D. Hallen, *Pure Appl. Chem.*, 1993, **65**, 1527.